CHINESE OPTICS LETTERS

Vol. 21, No. 1 | January 2023

All-solid-state far-UVC pulse laser at 222 nm wavelength for UVC disinfection

Qihui Luo (罗琪卉)[1,2], Jian Ma (马 剑)[1*], Miao Wang (王 淼)[1,2], Tingting Lu (陆婷婷)[1**], and Xiaolei Zhu (朱小磊)[1,2,3]

[1] Key Laboratory of Space Laser Communication and Detection Technology, Shanghai Institute of Optics and Fine Mechanics, Chinese Academy of Sciences, Shanghai 201800, China

[2] Center of Materials Science and Optoelectronics Engineering, University of Chinese Academy of Sciences, Beijing 100049, China

[3] Pilot National Laboratory for Marine Science and Technology, Qingdao 266237, China

*Corresponding author: majian@siom.ac.cn

**Corresponding author: tingting_lu@siom.ac.cn

Received April 18, 2022 | Accepted July 15, 2022 | Posted Online September 22, 2022

A 222 nm all-solid-state far-ultraviolet C (UVC) pulse laser system based on an optical parametric oscillator (OPO) and second-harmonic generation (SHG) using β-Ba_2BO_4 (BBO) crystals was demonstrated. Pumped by a Nd:$Y_3Al_5O_{12}$ laser with a repetition rate of 100 Hz at 355 nm, the maximum signal laser pulse energy of 1.22 mJ at 444 nm wavelength was obtained from the BBO-OPO system, corresponding to a conversion efficiency of 27.9%. The maximum output pulse energy of 164.9 μJ at the 222 nm wavelength was successfully achieved, corresponding to an SHG conversion efficiency of 16.2%. Moreover, the tunable output wavelength of UVC light from 210 nm to 252.5 nm was achieved.

Keywords: all-solid-state pulse laser; UVC disinfection; optical parametric oscillator; second-harmonic generation.
DOI: 10.3788/COL202321.011401

1. Introduction

In the past two years, due to the global pandemic of coronavirus disease 2019 (COVID-19), ultraviolet C (UVC, 200–280 nm) disinfection technology to inactivate viruses effectively has attracted extensive attention at home and abroad. Compared to other disinfection methods such as chemical disinfection and high temperature disinfection, UVC disinfection has the advantages of rapid effectiveness, broad spectrum, thoroughness, no resistance to drugs, no secondary pollution, and so on[1]. At present, the ultraviolet (UV) light sources used typically for disinfection mainly include low-pressure mercury lamps and UV light-emitting diodes (UV-LEDs)[2,3]. The main emission line of the low-pressure mercury lamp is 253.7 nm[3], which is effective in killing bacteria, while for UV-LED is mainly from 265 to 280 nm[4,5]. However, all of these wavelengths of conventional UVC disinfection methods can penetrate the skin stratum corneum and the ocular tear layer. Therefore, these germicidal UVC lights will do damage to human health, and even cause skin cancer and cataracts[6,7]. In 2017, Buonanno *et al.*[8] firstly reported, to the best of our knowledge, that far-UVC light (200–225 nm) could kill bacteria effectively, where they used a krypton chloride (KrCl) excimer lamp that produced 222 nm UV light to destroy a variety of microbes. Some studies suggest[8–11] that far-UVC light has the same sterilization effect as conventional UVC light. Nevertheless, far-UVC light cannot penetrate the cuticle of human skin, so it is harmless to human body. In 2020, Buonanno *et al.*[12] used low doses of 222 nm UV light to inactivate human coronaviruses, which showed that 222 nm UV light could kill coronaviruses effectively without damaging human health. All of the above show that 222 nm UV disinfection technology is a promising tool for virus elimination.

At present, the most common and widely studied device for emerging far-UVC is a KrCl excimer lamp. The central wavelength of the excimer lamp is 222 nm, and there are two emission peaks of 235 nm and 325 nm[13]. Therefore, special optical filters are needed to filter the bands above 230 nm in order to avoid the adverse effects on human health. In 2018, Ruhnke *et al.*[14] used a 445 nm gallium nitride (GaN) external cavity laser diode (LD) frequency doubling to generate 222.5 nm UV laser output, where a narrowband deep UV laser with an output power of 160 μW was achieved. In China, as early as the end of the 1980s, nonlinear frequency conversion techniques were adopted to produce UV lasers. In 1992, Fan *et al.*[15] reported a 196–228 nm tunable UV laser, which is produced by frequency conversion of β-Ba_2BO_4 (BBO) crystals from tunable output of a dye laser. In 2009, Zhang *et al.*[16] showed the widely tunable UV light from 170 to 232.5 nm by second-harmonic generation (SHG) of a frequency-doubled Ti:sapphire laser. However, up to now, there are few reports about compact, high peak-power all-solid-state lasers for UVC disinfection.

The all-solid-state laser has the advantages of small size, long lifetime, high beam quality, and narrow linewidth[17,18]. Crucially, it can emit a single wavelength without the need of spectral purification. Therefore, UVC lasers generated by all-solid-state lasers based on nonlinear frequency conversion technology are a new trend in UVC light sources. Furthermore, all-solid-state lasers working in pulse mode can emit pulses with very short pulse width and high peak power. Compared with ordinary UV light, pulsed UV light has a faster sterilization rate because it has stronger penetration ability and can induce the destruction reaction of the virus molecular structure more quickly. Consequently, to achieve the same bactericidal effect, pulsed UV light takes only a few pulses to complete, while ordinary UV light requires much longer working time[19].

In this paper, a 222 nm all-solid-state far-UVC laser based on an optical parametric oscillator (OPO) and SHG was presented. Pumped by a home-made *Q*-switched Nd:$Y_3Al_5O_{12}$ (Nd:YAG) laser with a repetition rate of 100 Hz, the pulse energy of 4.37 mJ at 355 nm was used as the pump source of the OPO. The maximum signal laser pulse energy of 1.22 mJ at 444 nm was achieved from this BBO-OPO system, corresponding to conversion efficiency of 27.9%. The pulse width of 444 nm was 8.2 ns with a spectrum linewidth of 0.05 nm. Using an SHG BBO cut at a Brewster angle, the maximum signal output energy of 164.9 μJ and SHG conversion efficiency of 16.2% at 222 nm were obtained. This compact, high peak-power far-UVC laser is expected to be used in fast UV physical disinfection devices, providing technical support for the fight against COVID-19.

2. Experimental Setup

The schematic diagram of the 222 nm all-solid-state far-UVC pulse laser system is shown in Fig. 1. The laser system is composed of three parts, which are a third-harmonic generation (THG)-based 355 nm UV laser unit, BBO-OPO unit, and UVC frequency doubling unit.

In the THG-based 355 nm laser unit, an LD pumped Nd:YAG laser operating at a repetition rate of 100 Hz offered fundamental laser pulses of 1064 nm, which were frequency-tripled to 355 nm by two LiB_3O_5 (LBO) crystals. The first one of the crystals was a type-I phase matching LBO crystal used for double frequency of 1064 nm, and the second one was a type-II phase matching LBO crystal used for sum frequency of 1064 nm and 532 nm.

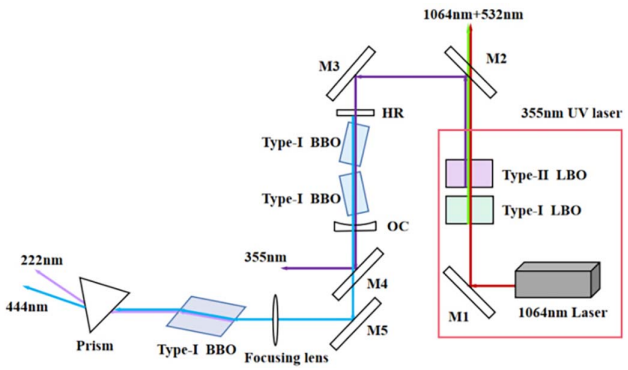

Fig. 1. Schematic diagram of the experimental setup.

The OPO unit pumped by the 355 nm laser was a plane-concave resonator with the length of 55 mm. This cavity was composed of a plane mirror and a concave output coupler (OC). The plane mirror was high-reflection (HR) coated at 430–460 nm and anti-reflection (AR) coated at 355 nm and 1600–2000 nm, while the concave OC with the curvature radius of 1000 mm was partly reflection coated at 430–460 nm with transmission of 35% around 440 nm and AR coated at 355 nm and 1600–2000 nm. Two 5 mm × 3 mm × 10 mm type-I phase matching BBO crystals cut at $\theta = 29.6°$, $\phi = 90°$ were inserted in this OPO as parametric crystals. In order to compensate the walk-off effect, two BBO crystals were placed cross symmetrically, similar to what was mentioned by Zhang *et al.*[20]. Wavelength tuning output of the OPO could be obtained by rotating those two BBO crystals symmetrically.

The 444 nm laser beam from the OPO was then focused by convex lens $f = 125$ mm, which is used as the pump beam for frequency doubling. The type I BBO crystal, with dimensions of 4 mm × 4 mm × 7 mm, was used for SHG, and its two end-faces are cut at Brewster angles of $\theta_B = 59.3°$. The fundamental laser at 444 nm and the SHG laser at 222 nm were separated by a fused quartz prism. The loss of M5 was 16%.

3. Results and Discussion

In this laser system, the Nd:YAG laser provided a maximum pulse energy of 10.3 mJ, and the pulse energy of 355 nm was around 4.37 mJ, the pulse width was about 10 ns, and the beam diameter was 1 mm. Consequently, the maximum peak-power density of the 355 nm laser was around 55.6 MW/cm^2.

The signal output pulse energy of the OPO at 444 nm as a function of the pump pulse energy input is shown in Fig. 2. The output energy of the 444 nm laser increased linearly with the increasing pump energy of the 355 nm laser, and no saturation was observed. The maximum output pulse energy of 1.22 mJ at 444 nm wavelength was obtained with 4.37 mJ pump input, corresponding to a conversion efficiency of 27.9% and a slope efficiency of 39%.

The maximum conversion efficiency η in a singly resonant pulsed OPO is determined by[21]

$$\eta = 0.9 \times \frac{1-R}{1-R\times(1-\delta_{\text{scat}})} \times \frac{(\ln N)^{2.33}}{N}, \tag{1}$$

where R is the reflectivity of the concave OC, δ_{scat} is the cavity scattering loss, and N is the ratio of the pump density to the threshold pump density. In this OPO system, the threshold pump density was about 16.6 MW/cm^2, so $N = 3.35$ when the maximum peak-power density of the pump pulse was 55.6 MW/cm^2. Taking δ_{scat} as 0.2 into calculation, η could be

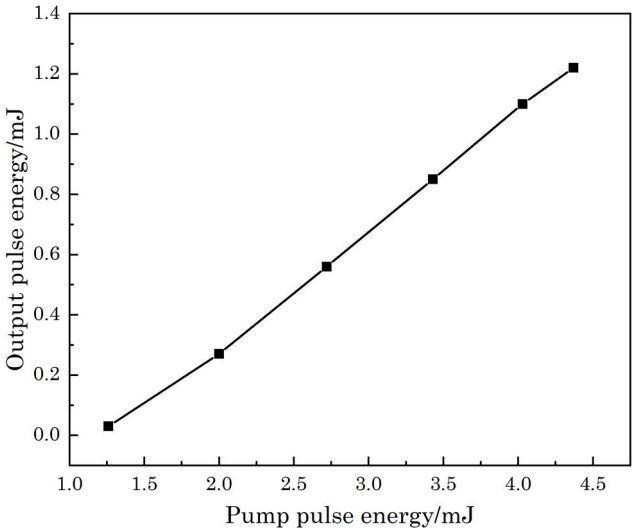

Fig. 2. Output pulse energy of the OPO at 444 nm as a function of the pump pulse energy.

calculated to be 30.5% theoretically, which was bigger than the result from the experiment.

Figure 3 shows the temporal profile of the 444 nm laser pulse output from this BBO OPO system, which was detected by Hamamatsu biplanar phototubes R1193U-52 and recorded by a Tektronix oscilloscope MDO4034C. The pulse duration of the signal at 444 nm was measured as 8.2 ns, which was less than 10 ns of the pump pulse duration at 355 nm.

The near-field beam profile of the 444 nm laser with a maximum output detected by a Spiricon silicon CCD camera (SP620) is shown in Fig. 4. The 444 nm laser beam was nearly circular and well-proportioned with the size about 1.45 mm × 1.64 mm and the corresponding far-field divergence of $\theta_x = 3.27$ mrad and $\theta_y = 3.75$ mrad. The M^2 of the 444 nm laser beam was measured by a Spiricon laser beam analyzer (M^2-200s), as shown in Fig. 5. The M^2 factors in the x and y directions were 4.44 and 6.60, respectively. In this BBO-OPO system, the x and y directions represented the parallel and

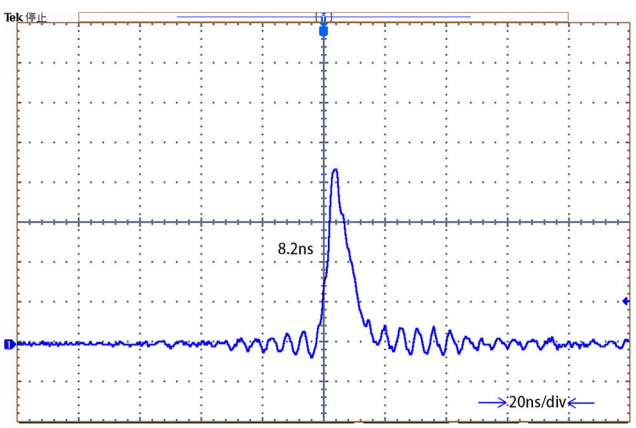

Fig. 3. Pulse temporal profile of the 444 nm laser.

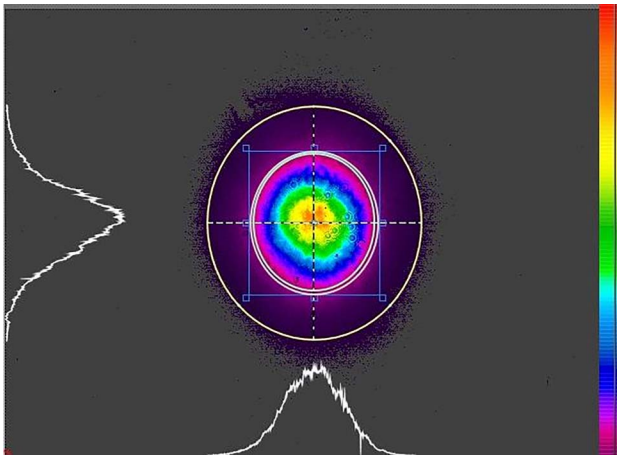

Fig. 4. Intensity distribution profile of 444 nm laser beam.

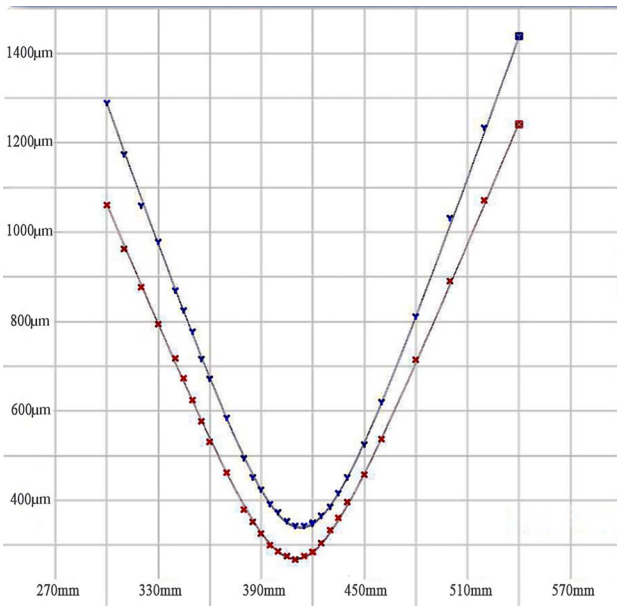

Fig. 5. M^2 factors measured for the 444 nm laser beam.

perpendicular walk-off orientation of the pump laser, respectively. It could be found that the departure effect in the crystals of the pump beam was compensated effectively by adopting a cross symmetrical placing of the two BBO crystals.

Figure 6 shows the output signal laser spectrum of the OPO, which was measured by the Yokogawa optical spectrum analyzer AQ6373B with the measurement resolution of 0.02 nm. The central wavelength was 444.01 nm, and the spectrum width was less than 0.05 nm.

From the above results, it could be calculated that the peak-power density of the OPO output 444 nm laser was 8.4 MW/cm^2. After passing through the focusing lens, the peak-power density near the focal plane was increased to about 82.2 MW/cm^2, so the efficiency of SHG could be improved greatly. The output energy of the 222 nm pulse as a function of the fundamental 444 nm pulse energy is displayed in

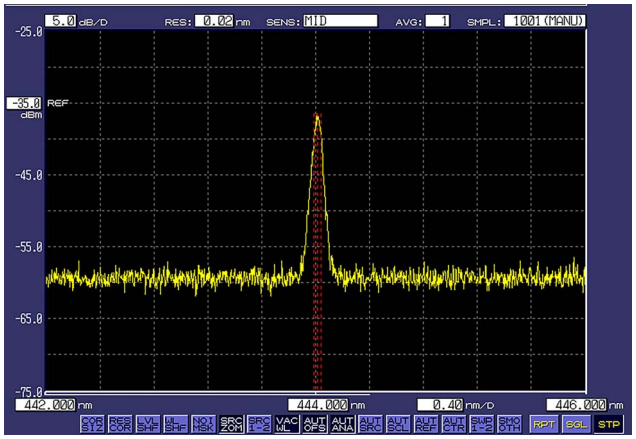

Fig. 6. Output laser spectrum of the OPO at 444 nm.

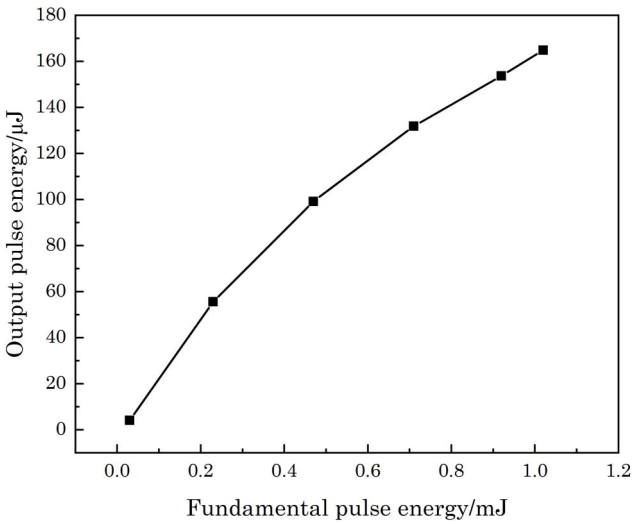

Fig. 7. Output pulse energy of SHG at 222 nm as a function of the fundamental pulse energy.

Fig. 7. The 222 nm laser output energy increased with the pump energy increasing. The maximum 222 nm laser pulse energy of 164.9 μJ was achieved, corresponding to the SHG conversion efficiency of 16.2%.

The spectrum of the 222 nm laser pulse was detected by an Ocean optic spectrometer (Maya2000Pro), as shown in Fig. 8. It could be read that the central wavelength of the SHG output laser was around 222.14 nm.

The pulse temporal profile of the 222 nm laser pulse was also detected by phototube R1193U-52 and recorded by a Tektronix oscilloscope MDO4034C, as shown in Fig. 9. The pulse duration was about 7.9 ns, which was a bit less than the fundamental pulse duration, and the peak-power density of 222 nm can be calculated as 13.7 MW/cm^2, corresponding to the energy density of 108 mJ/cm^2; it was much higher than the dose of 2 mJ/cm^2, which is needed to inactivate the virus[22].

Since a wide tuning range of the OPO can be achieved by symmetrically rotating those two BBO crystals, a tunable output in

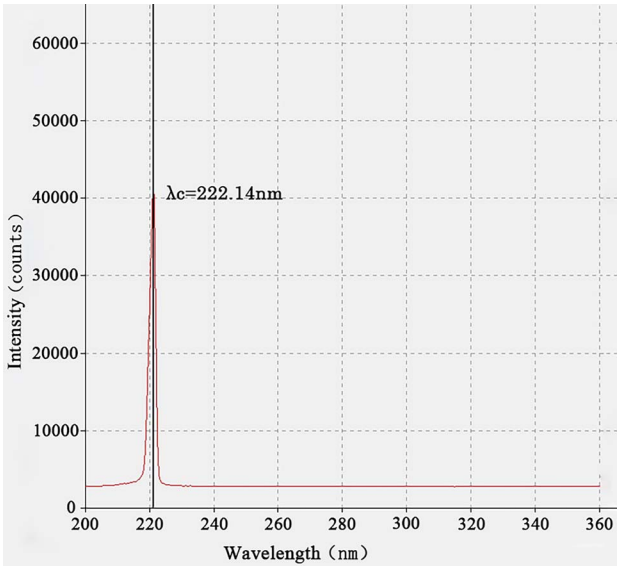

Fig. 8. Spectrum of the 222 nm laser.

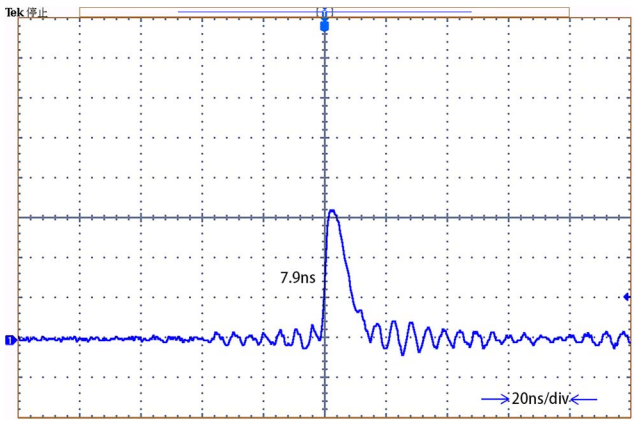

Fig. 9. Pulse temporal profile of the 222 nm laser.

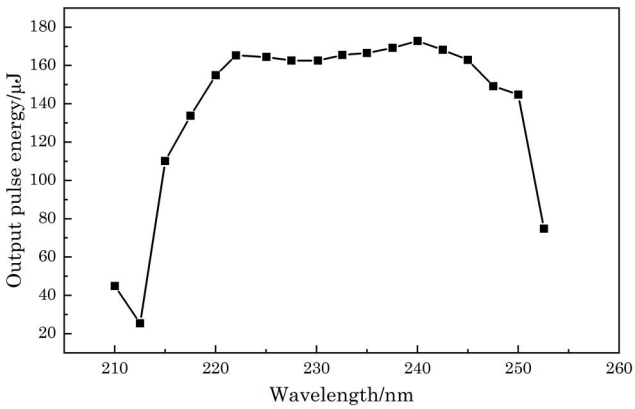

Fig. 10. Tunable output in UVC spectral range.

UVC was demonstrated in this experimental setup. Figure 10 shows the detected tuning output curve with a range of 42.5 nm from 210 nm to 252.5 nm, and the maximum UVC pulse energy was above 160 μJ.

4. Conclusion

In summary, a 222 nm all-solid-state far-UVC laser based on BBO-OPO and BBO-SHG was demonstrated. At a pulse repetition rate of 100 Hz, with maximum pump pulse energy of 4.37 mJ at 355 nm, 1.22 mJ pulse energy at 444 nm wavelength was obtained from the BBO-OPO system, corresponding to a conversion efficiency of 27.9%, and, finally, 164.9 μJ pulse energy at the 222 nm wavelength was detected, corresponding to an SHG optical-to-optical conversion efficiency of 16.2%. The laser pulse energy density at 222 nm is sufficient for virus inactivation. Such a compact, high peak-power far-UVC laser has a great prospect for the applications of UV disinfection.

Acknowledgement

This work was supported by the Natural Science Foundation of Shanghai (No. 19YF1453600), the Key Task Project in Scientific and Technological Research on Social Development of Shanghai (No. 20dz1206502), the Strategic Priority Research Program of the Chinese Academy of Sciences (No. XDA22000000), and the Major Program of the National Natural Science Foundation of China (No. 61991453).

References

1. B. Ma, P. M. Gundy, C. P. Gerba, M. D. Sobsey, and K. G. Linden, "UV inactivation of SARS–CoV–2 across the UVC spectrum: KrCl excimer, mercury-vapor, and light–emitting–diode (LED) sources," Appl. Environ. Microbiol. **87**, e01532 (2021).
2. N. M. Hull and K. G. Linden, "Synergy of MS_2 disinfection by sequential exposure to tailored UV wavelengths," Water Res. **143**, 292 (2018).
3. S. E. Beck, R. A. Rodriguez, K. G. Linden, T. M. Hargy, T. C. Larason, and H. B. Wright, "Wavelength dependent UV inactivation and DNA damage of adenovirus as measured by cell culture infectivity and long range quantitative PCR," Environ. Sci. Technol. **48**, 591 (2014).
4. K. G. Linden, N. Hull, and V. Speight, "Thinking outside the treatment plant: UV for water distribution system disinfection," Acc. Chem. Res. **52**, 1226 (2019).
5. S. E. Beck, H. Ryu, L. A. Boczek, J. L. Cashdollar, K. M. Jeanis, J. S. Rosenblum, O. R. Lawal, and K. G. Linden, "Evaluating UV-C LED disinfection performance and investigating potential dual-wavelength synergy," Water Res. **109**, 207 (2017).
6. S. Zaffifina, V. Camisa, M. Lembo, M. R. Vinci, M. G. Tucci, M. Borra, A. Napolitano, and V. Cannatã, "Accidental exposure to UV radiation produced by germicidal lamp: case report and risk assessment," Photochem. Photobiol. **88**, 1001 (2012).
7. R. B. Setlow, E. Grist, K. Thompson, and A. D. Woodhead, "Wavelengths effective in induction of malignant melanoma," Proc. Natl Acad. Sci. USA **90**, 6666 (1993).
8. M. Buonanno, B. Ponnaiya, D. Welch, M. Stanislauskas, G. Randers-Pehrson, L. Smilenov, F. D. Lowy, D. M. Owensb, and D. J. Brennera, "Germicidal efficacy and mammalian skin safety of 222–nm UV light," Radiat. Res. **187**, 493 (2017).
9. M. Buonanno, G. Randers-Pehrson, A. W. Bigelow, S. Trivedi, F. D. Lowy, H. M. Spotnitz, S. M. Hammer, and D. J. Brenner, "207–nm UV light–a promising tool for safe low-cost reduction of surgical site infections. I: *in vitro* studies," PLoS ONE **8**, e76968 (2013).
10. M. Buonanno, M. Stanislauskas, B. Ponnaiya, A. W. Bigelow, G. Randers-Pehrson, Y. Xu, I. Shuryak, L. Smilenov, D. M. Owens, and D. J. Brenner, "207-nm UV light-a promising tool for safe low-cost reduction of surgical site infections. II: *in vivo* safety studies," PLoS ONE **11**, e0138418 (2016).
11. B. Ponnaiya, M. Buonanno, D. Welch, I. Shuryak, and D. J. Brenner, "Far–UVC light prevents MRSA infection of superficial wounds *in vivo*," PLoS ONE **13**, e0192053 (2018).
12. M. Buonanno, D. Welch, I. Shuryak, and D. J. Brenner, "Far–UVC light (222 nm) efficiently and safely inactivates airborne human coronaviruses," Sci. Rep. **10**, 10285 (2020).
13. J. Zhanga and I. W. Boyd, "Efficient excimer ultraviolet sources from a dielectric barrier discharge in rare-gas/halogen mixtures," J. Appl. Phys. **80**, 633 (1996).
14. N. Ruhnke, A. Müller, B. Eppich, M. Maiwald, B. Sumpf, G. Erbert, and G. Tränkle, "Compact deep UV system at 222.5 nm based on frequency doubling of GaN laser diode emission," IEEE Photonics Technol. Lett. **30**, 289 (2018).
15. Q. Fan, Z. Lu, B. Wu, and Z. Hong, "Generation of UV radiation of 196–228 nm with BBO crystal," Acta Opt. Sin. **12**, 403 (1992).
16. X. Zhang, Z. Wang, G. Wang, Y. Zhu, Z. Xu, and C. Chen, "Widely tunable and high-average-power fourth-harmonic generation of a Ti:sapphire laser with a $KBe_2BO_3F_2$ prism-coupled device," Opt. Lett. **34**, 1342 (2009).
17. M. Zhao, C. Wang, Q. Hao, Z. Zou, J. Liu, X. Fan, and L. Su, "High single-pulse energy passively *Q*-switched laser based on Yb, Gd:SrF_2 crystal," Chin. Opt. Lett. **18**, 101401 (2020).
18. Y. Zhang, J. Zou, W. Zheng, K. Feng, B. Xu, and Z. Yu, "Watt-level continuous-wave intracavity frequency-doubled Pr:YLF-LBO laser at 320 nm," Chin. Opt. Lett. **19**, 091406 (2021).
19. C. Wang, L. Hu, and J. Long, "The mechanism and application prospect of pulsed UV strong light sterilization technology," Chin. J. Disinfect. **33**, 1104 (2016).
20. J. Zhang, J. Ma, T. Lu, D. Liu, X. Zhu, and W. Chen, "Compact wavelength tunable output around 440 nm pulsed laser for oceanic lidar application," Opt. Commun. **485**, 126706 (2021).
21. E. Granot, S. Pearl, and M. M. Tilleman, "Analytical solution for a lossy singly resonant optical parametric oscillator," J. Opt. Soc. Am. B **17**, 381 (2000).
22. D. Welch, M. Buonanno, V. Grilj, I. Shuryak, C. Crickmore, A. W. Bigelow, G. Randers-Pehrson, G. W. Johnson, and D. J. Brenner, "Far-UVC light: a new tool to control the spread of airborne-mediated microbial diseases," Sci. Rep. **8**, 2752 (2018).